

# Dynamic analysis of metro vehicle traveling on a high-pier viaduct under crosswind in Chongqing

Yunfei Zhang<sup>1</sup>, Jun Li<sup>\*1,2</sup>, Zhaowei Chen<sup>1,2</sup> and Xiangyang Xu<sup>1,2</sup>

<sup>1</sup>School of Mechatronics and Vehicle Engineering, Chongqing Jiaotong University, Chongqing 400074, China

<sup>2</sup>Chongqing Key Laboratory of Integration and Control for Urban Rail Transit Vehicle System, Chongqing 400074, China

(Received October 19, 2018, Revised April 7, 2019, Accepted May 11, 2019)

**Abstract.** Due to the rugged terrain, metro lines in mountain city across numerous wide rivers and deep valleys, resulting in instability of high-pier bridge and insecurity of metro train under crosswind. Compared with the conditions of no-wind, crosswind triggers severer vibration of the dynamic system; compared with the short-pier viaduct, the high-pier viaduct has worse stability under crosswind. For these reasons, the running safety of the metro vehicle traveling on a high-pier viaduct under crosswind is analyzed to ensure the safe operation in metro lines in mountain cities. In this paper, a dynamic model of the metro vehicle-track-bridge system under crosswind is established, in which crosswind loads model considering the condition of wind zone are built. After that, the evaluation indices and the calculation parameters have been selected, moreover, the basic characteristics of the dynamic system with high-pier under crosswind are analyzed. On this basis, the response varies with vehicle speed and wind speed are calculated, then the corresponding safety zone is determined. The results indicate that, crosswind triggers drastic vibration to the metro vehicle and high-pier viaduct, which in turn causes running instability of the vehicle. The corresponding safety zone for metro vehicle traveling on the high-pier is proposed, and the metro traffic on the high-pier bridge under crosswind should not exceed the corresponding limited vehicle speed to ensure the running safety.

**Keywords:** running safety; crosswind; high-pier viaduct; metro vehicle-track-bridge interaction; mountain city

## 1. Introduction

Chongqing is a typical mountain city in Southwest China, whose rail transit is increasingly developing. Nevertheless, due to the sinister terrain, the metro lines across numerous wide rivers and deep valleys, causing a large proportion of high-pier viaducts, and the height of pier is even higher than 100 meters. Compared with the underground line in plain city, the elevated line in mountain city is severely attacked by environmental gusts, which induces the drastic vibration of the dynamic system, especially at the turn of summer and autumn. Besides, compared with the short-pier viaduct, the high-pier viaduct has worse stability under crosswind. Crosswind induces the strong vibration of the high-pier and the beam, which causes the intensified vibration of the track structure by the track-bridge interaction. Then the vibration transmits to the car body by wheel-rail interaction, that in turn triggers running instability of metro train to be derailed or overturn in serious cases, which results in loss of running safety or traffic disruption.

By now, many studies have paid their attention to the wind-train-bridge (WTB) coupled system, and many beneficial suggestions have been proposed. In the authors' opinion, these studies on the WTB interaction can be classified into the following three categories by research method: a) wind tunnel tests; b) analytical approaches; c)

computer fluid dynamics.

Wind tunnel tests (WTT) plays an essential role in studying the WTB system (Cai *et al.* 2015). Protection effect of wind barrier on running safety of train under crosswind has been analyzed by WTT (Olmos and Astiz 2018, Chen *et al.* 2015, He *et al.* 2016, Xiang *et al.* 2018). In addition, the characteristics of single running train or the meeting of two trains on bridges under wind loads have been researched (Li *et al.* 2014, Niu *et al.* 2017, Li *et al.* 2013, Cheli *et al.* 2011).

Analytical approaches are used to study the WTB interaction through building an analytical model and investigating the concerned parameters and responses of the structure based upon the knowledge of structural dynamics and fluid mechanics (Cai *et al.* 2015, Cai *et al.* 2019). The running safety or stability analysis of the WTB system has been finished in a slice of works (Carsten *et al.* 2015), the non-linear model for WTB interaction was built by Olmos and Astiz (2018), in addition, running safety on the Tsing Ma Bridge was analyzed by Guo *et al.* (2011).

Computer Fluid Dynamics (CFD), which is an efficient tool to reveal the aerodynamic phenomena of running train and bridge structures under wind (Cai *et al.* 2015), for instance, Weinman *et al.* (2018) assessed the effect of mesh refinement by comparing CFD with WTT.

However, few studies pay attention to the running safety of the metro vehicle-bridge system with high-pier under crosswind. For this reason, this paper analyzes the running safety of the metro vehicle over the high-pier viaduct under crosswind to ensure the safe operation in metro lines in mountain cities. Firstly, the dynamic model of the metro vehicle-track-bridge system under crosswind is established

---

\*Corresponding author, Professor  
E-mail: [cqleejun@163.com](mailto:cqleejun@163.com)

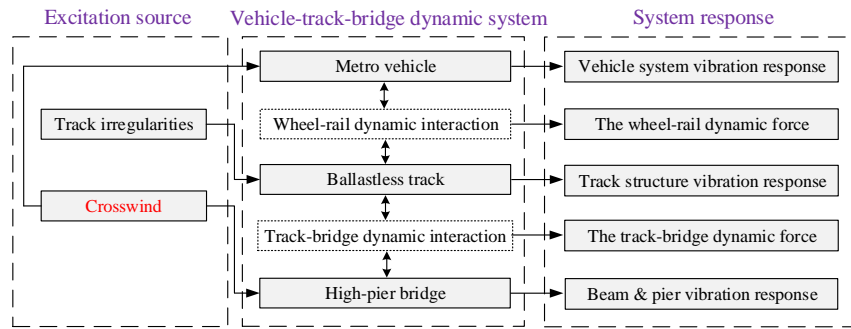
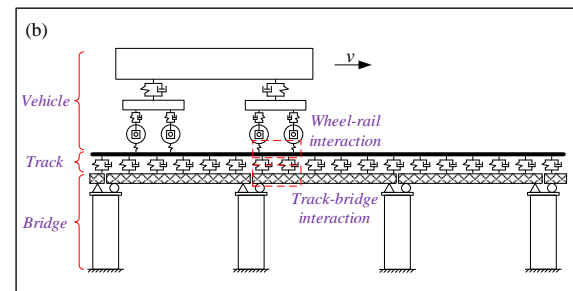


Fig. 1 Dynamic interaction principle of metro vehicle-track-bridge under crosswind



(a) the viaduct and metro vehicle of Chongqing Rail Transit Line-10 (CRT10)



(b) dynamic model of the metro vehicle-track-bridge system with high-pier viaduct

Fig. 2 Dynamic model of the vehicle-track-bridge system

in Section 2. Then, crosswind loads model considering the condition of wind zone is built in the next section. On this basis, the basic characteristics of the dynamic system with high-pier under crosswind are analyzed in Section 4. After that, the safety zone for metro vehicle traveling on the high-pier viaduct under crosswind is determined in the last section. Finally, some crucial conclusions are reached in the end of the work.

Several highlights in this paper are listed below:

- A dynamic model of the metro train-track-bridge system subjected to crosswind in mountain city is established;
- Considering the condition of wind zone in mountain city, crosswind loads for high-pier bridge and metro vehicle are described;
- Running safety of the metro vehicle over a high-pier viaduct under crosswind is researched, in which the corresponding safety zone is determined.

## 2. Dynamic model of metro vehicle-track-bridge system under crosswind

According to the actual construction of Chongqing Rail Transit (CRT), a detailed dynamic model of the vehicle-track-bridge system is established. In the dynamic model, metro vehicle, ballastless track and high-pier bridge are considered as three subsystems, which are coupled through wheel-rail interaction and track-bridge interaction. Besides, the dynamic equations are calculated by the Newmark- $\beta$

numerical integration method. Dynamic interaction principle of metro vehicle-track-bridge under crosswind is shown in Fig. 1 (Zhai *et al.* 2011).

### 2.1 Metro vehicle sub-model

Based on the actual condition of metro vehicles of CRT, as shown in Fig. 2, the following assumptions are adopted for the vehicle model. The metro vehicle runs at a constant speed on the windward side track of the double-line bridge. Then, the vehicle consists of a car body, two bogies, four wheelsets and eight axle-boxes, which are all rigid bodies. In the meantime, six degrees of freedom (DOFs) are taken into consideration for each rigid body except the axle-boxes, describing stretch, bounce, sway, roll, yaw, and pitch motions, in which total 50 DOFs are considered. Meanwhile, the viscous dampers and linear springs are adopted in primary and secondary suspension systems to build the vehicle sub-model. The detailed equations of motion of all the parts can be found in Zhai *et al.* (2013).

### 2.2 Ballastless track sub-model

The rails are modeled as Euler beams, which discretely supported by fasteners and are simulated as linear spring-damping force elements. Meanwhile, the track slab and the bridge deck are casted as one, as shown in Fig. 2(b). And three DOFs of each rail are taken into account, describing vertical motion, lateral motion, and torsional motion, and the motion of the rail are given as (Chen *et al.* 2015)



$$\begin{cases} F_x = -f_{11} \cdot \varepsilon_x \\ F_y = -f_{22} \cdot \varepsilon_y - f_{23} \cdot \varepsilon_\phi \\ M_z = -f_{23} \cdot \varepsilon_y - f_{33} \cdot \varepsilon_\phi \end{cases} \quad (8)$$

where  $f_{ij}$  ( $i, j = 1, 2, 3$ ) is creep coefficient,  $\varepsilon_x$ ,  $\varepsilon_y$  and  $\varepsilon_\phi$  show the definitions of the longitudinal, lateral and spin creepage.

### 2.5 Track-bridge dynamic interaction

Track-bridge dynamic interaction is adopted to investigate the track-bridge interaction forces, which is illustrated in Fig. 4.

In the solution for track-bridge vertical force, the left and right vertical track-bridge interaction force  $F_{rVLi}(t)$  and  $F_{rVRi}(t)$  under the  $i$ th fastener can be described as

$$\begin{cases} F_{rVLi} = K_{fV}(z_{rLi} - z_{bV} + \phi_b d) + C_{fV}(\dot{z}_{rLi} - \dot{z}_{bV} + \dot{\phi}_b d) \\ F_{rVRi} = K_{fV}(z_{rRi} - z_{bV} - \phi_b d) + C_{fV}(\dot{z}_{rRi} - \dot{z}_{bV} - \dot{\phi}_b d) \end{cases} \quad (9)$$

where among them,  $K_{fV}$  and  $C_{fV}$  are the fastener's vertical stiffness and damping;  $z_{rLi}$  and  $z_{rRi}$  are the vertical displacements of the left and right rails at the  $i$ th fastener position;  $z_{bV}$  and  $\phi_b$  are the vertical displacements and torsional angles of the bridge section centroid;  $d$  represents half of the track gauge.

The left and right lateral track-bridge interaction forces are described as

$$\begin{cases} F_{rLLi} = K_{fL}(y_{rLi} - y_{bL} - \phi_b H_b) + C_{fL}(\dot{y}_{rLi} - \dot{y}_{bL} - \dot{\phi}_b H_b) \\ F_{rLRi} = K_{fL}(y_{rRi} - y_{bL} - \phi_b H_b) + C_{fL}(\dot{y}_{rRi} - \dot{y}_{bL} - \dot{\phi}_b H_b) \end{cases} \quad (10)$$

where  $K_{fL}$  and  $C_{fL}$  are the lateral stiffness and damping of fasteners;  $y_{rLi}$  and  $y_{rRi}$  are the lateral displacements of the left and right rails at the  $i$ th fastener position;  $y_{bL}$  is the lateral displacement of the bridge section centroids;  $H_b$  represents the bridge section centroid to the bridge The distance from the surface.

### 2.6 Numerical solution

In order to improve the efficiency of computer computing and ensure the stability of calculation, academician Zhai proposed the Newmark- $\beta$  implicit integral method (Zhai method, 1996) to solve the equations of vehicle-track submodel (Li *et al.* 2013). In this work, Newmark- $\beta$  integral method is adopted to solve the established dynamic equations, whose integral expression is

$$\begin{cases} X_{n+1} = X_n + \dot{X}_n \Delta t + (1/2 + \psi) \ddot{X}_n \Delta t^2 - \psi \ddot{X}_{n-1} \Delta t^2 \\ \dot{X}_{n+1} = \dot{X}_n + (1 + \varphi) \ddot{X}_n \Delta t - \varphi \ddot{X}_{n-1} \Delta t \end{cases} \quad (11)$$

where  $X$ ,  $\dot{X}$  and  $\ddot{X}$  are the generalized matrix displacement, velocity, acceleration of the dynamic system, respectively;  $\varphi$ ,  $\psi$  are the integral parameters;  $\Delta t$  is the time integration step length.

The mixed explicit-implicit integration method can be conducted according to the procedure in Fig. 5 (Chen *et al.* 2019).

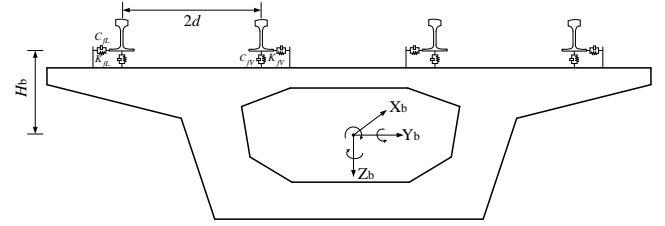


Fig. 4 Track-bridge dynamic interaction

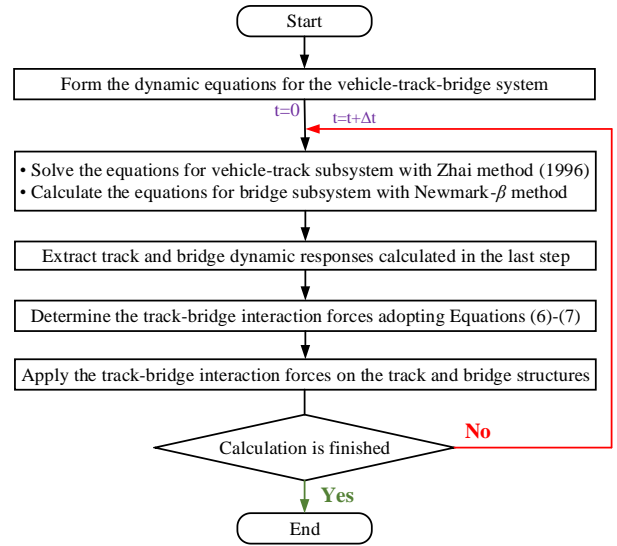


Fig. 5 Process of the mixed explicit-implicit integration method

## 3. Crosswind loads model

Crosswind loads for the high-pier, the box-girder and the car body of are described sequentially in this section.

### 3.1 Numerical simulation of crosswind velocity time histories

According to the actual statistical meteorological data in Chongqing, a detailed crosswind model is built, as shown in Fig. 6, in which the following assumptions are adopted:

- Crosswind in this paper is described as a natural unsteady gust with step change; meanwhile, the process of metro vehicle crossing over the wind zone is divided into three stages: a) entering stage; b) crossing stage; c) leaving stage.
- The crosswind speed is gradient along the elevation of the pier, which does not change along the bridge deck. Besides, crosswind only works on the car body, the box girder and the high-pier. The mean wind speeds for the vehicle, the bridge deck and the pier top are equal.

Fluctuating gust action is a random process, and the value of wind load changes constantly and is unpredictable. It cannot be completely described by time function, but it can be analyzed by probability theory and random vibration

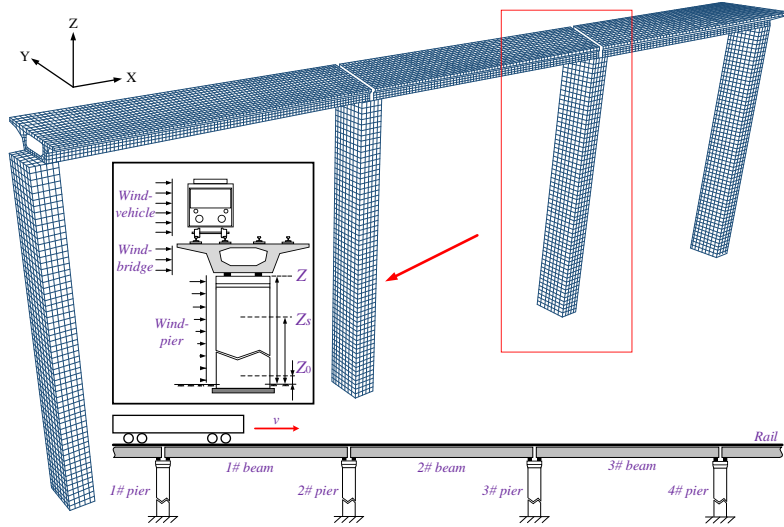


Fig. 6 Finite element model of the high-pier bridge and the schematic of crosswind for the dynamic system

theory. According to wind records, fluctuating wind can be considered as Gaussian process and stationary random process. The harmonic superposition method (HSM) is adopted to simulate. The numerical simulation procedure is shown in Fig. 7.

The power spectral density (PSD) function with  $n$  smooth Gaussian processes ( $v_j(t)$  ( $j = 1, 2, \dots, n$ )) with zero mean value is (Cheli *et al.* 2018, Chen *et al.* 2015)

$$S_{jk}(\omega) = \begin{bmatrix} S_{11}(\omega) & S_{12}(\omega) & \cdots & S_{1n}(\omega) \\ S_{21}(\omega) & S_{22}(\omega) & \cdots & S_{2n}(\omega) \\ \vdots & \vdots & \ddots & \vdots \\ S_{n1}(\omega) & S_{n2}(\omega) & \cdots & S_{nm}(\omega) \end{bmatrix} \quad (12)$$

where  $S_{jk}(\omega)$  ( $j = 1, 2, \dots, n; k = 1, 2, \dots, n$ ) is the Fourier transform (FT) of the correlation function.

According to Cholesky's decomposition method,  $S_{jk}(\omega)$  is decomposed as

$$S_{jk}(\omega) = H(\omega)H^*(\omega)^T \quad (13)$$

where  $H(\omega)$  is a down triangular matrix,  $H^*(\omega)^T$  is the matrix transpose of  $H(\omega)$ .

$$H(\omega) = \begin{bmatrix} H_{11}(\omega) & 0 & \cdots & 0 \\ H_{21}(\omega) & H_{22}(\omega) & \cdots & 0 \\ \vdots & \vdots & \ddots & \vdots \\ H_{n1}(\omega) & H_{n2}(\omega) & \cdots & H_{nm}(\omega) \end{bmatrix} \quad (14)$$

where the  $S_{jk}(\omega)$  is the multidimensional random processes, the numerical simulation of fluctuating wind velocity  $v_j(t)$  histories are described as

$$v_j(t) = \sum_{k=1}^j \sum_{l=1}^N |H_{jm}(\omega_l)| \cdot \sqrt{2\Delta\omega} \cdot \cos[\omega_l t + \psi_{jm}(\omega_l) + \theta_{ml}] \quad (15)$$

$j = 1, 2, 3, \dots, n$

where  $\Delta\omega = (\omega_u - \omega_k)/N$  is the increment of frequency,  $\omega_u$  and  $\omega_k$  are the upper and lower limits of frequency;  $|H_{jm}(\omega_l)|$  is the matrix module of  $H(\omega)$ ;  $\psi_{jm}(\omega_l)$  is the phase angle between two points,  $l = 1, 2, 3, \dots, N$ ;  $\theta_{ml}$  is random numbers uniformly distributed between 0 and  $2\pi$ .  $\omega_l = \omega_k + (l-1/2)\Delta\omega$  is the increasing variable of frequency.

Davenport spectrum is adopted in this paper according to 'Fundamental code for design on railway bridge and culvert TB 10002.1-2005'.

$$S_u(n) = \frac{4Kr\bar{U}_{10}^{-2}}{n} \cdot \frac{x_0^2}{(1+x_0^2)^{4/3}} \quad (16)$$

where  $x_0 = 1200n/\bar{U}_{10}$ ;  $\bar{U}_{10}$  is the average wind speed at ground base height of 10 m;  $n$  is the frequency of wind (1/s);  $K_r$  is the coefficient of friction at 10 meters.

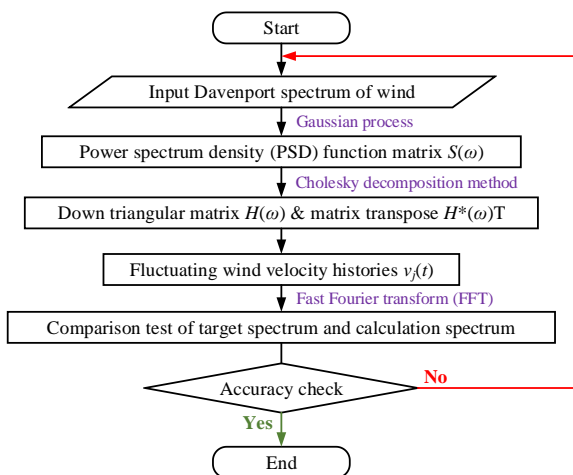


Fig. 7 Numerical simulation procedure of fluctuating wind

Crosswind changes along the gradient, whose speed is reduced by the frictional resistance when air flow is close to the ground. On the contrary, the higher air flow away from the ground, the less energy loss is, higher wind speed is. Generally, the wind pressure at the standard height ( $z = 20$  m) is adopted in ‘*Fundamental code for design on railway bridge and culvert TB 10002.1-2005*’. According to the standard, the exponential law is suitable for the upper friction layer, while the logarithmic law is suitable for the lower friction layer near the ground.

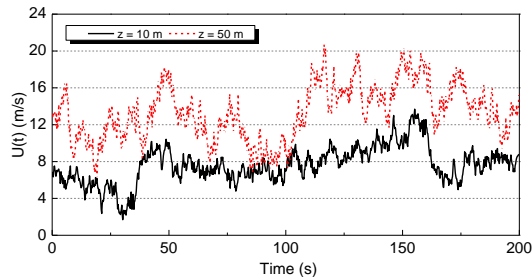
$$\begin{cases} \bar{U}_{zu} = \bar{U}_s(z/z_s)^\alpha \\ \bar{U}_{zd} = \bar{U}_s(\lg z - \lg z_0)/(\lg z_s - \lg z_0) \\ U(t) = \bar{U}(z) + v_j(t) \end{cases} \quad (17)$$

where  $\bar{U}_{zu}$  and  $\bar{U}_{zd}$  are the average wind speed (m/s) at the height  $z$  of the upper and lower friction layers;  $\bar{U}_s$  is the average wind speed (m/s) at the standard height  $z_s$ ;  $\alpha$  is the ground roughness index, which is set to 0.30;  $z_0$  is the height at which the wind speed is reduced to 0.

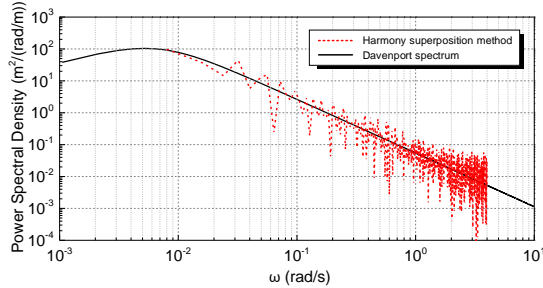
On this basis, the wind velocities along the bridge deck and the pier are generated, as shown in Fig. 8.

As can be seen from Fig. 8(a), for instance, while mean crosswind speed of standard height is 8 m/s, simulated time histories of crosswind at the bridge mid-span ( $z = 50$  m) and lower friction layers height of the pier ( $z = 10$  m) are given.

Meanwhile, as shown in Fig. 8(b), the calculated spectrum is floating on both sides of the target spectrum in the simulation process, that conforms to the curve rule of the target spectrum and is consistent with the target spectrum, which indicates the HSM is credible.

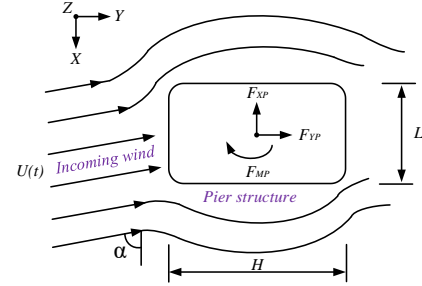


(a) Numerical simulation of fluctuating wind

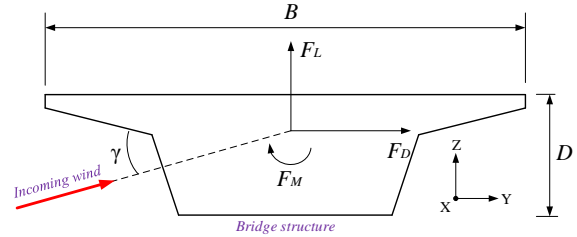


(b) The target spectrum and calculation spectrum

Fig. 8 Numerical simulation of fluctuating wind



(a) Aerodynamic forces on the high-pier and sign conventions



(b) Aerodynamic forces on the bridge structure and sign conventions

Fig. 9 Crosswind loads for high-pier bridge

### 3.2 Crosswind load for high-pier viaduct

The pier structure is affected by natural wind force (per unit height) with an attack angle  $\alpha$  on its section (Guo *et al.* 2010, Weinman *et al.* 2018), which is shown in Fig. 9.

Tri-component forces of the vehicle-bridge system under natural wind are shown as

$$\begin{cases} F_{YP}(t) = 0.5\rho \cdot U(t)^2 C_{YP}(\alpha)L \\ F_{XP}(t) = 0.5\rho \cdot U(t)^2 C_{XP}(\alpha)H \\ F_{MP}(t) = 0.5\rho \cdot U(t)^2 C_{MP}(\alpha)H^2 \end{cases} \quad (18)$$

where  $F_{YP}$ ,  $F_{XP}$ ,  $F_{MP}$  are the Y-Pier-Force, X-Pier-Force and Pier-Moment, respectively;  $\rho$  is the air density;  $L$  is the width of pier section;  $C_{YP}$ ,  $C_{XP}$ ,  $C_{MP}$  are the aerodynamic coefficients related to section shape and flow direction. The coefficients can be obtained from WTT or CFD simulation

Wind loads (per unit length) for the box girder, shown in Fig. 9, can be expressed as follows

$$\begin{cases} F_{DB}(t) = 0.5\rho \cdot U(t)^2 C_{DB}(\gamma)D \\ F_{LB}(t) = 0.5\rho \cdot U(t)^2 C_{LB}(\gamma)B \\ F_{MB}(t) = 0.5\rho \cdot U(t)^2 C_{MB}(\gamma)B^2 \end{cases} \quad (19)$$

where ‘DB’ is the drag wind load on bridge, ‘LB’ is the lift wind load on bridge, ‘MB’ is the moment wind load on bridge, respectively;  $B$  is the width of body along the mean wind;  $D$  is the height of bridge section.

In addition, the functions of the aerodynamic coefficient,  $C_{YP}$ ,  $C_{XP}$ ,  $C_{MP}$ ,  $C_{DB}$ ,  $C_{LB}$ ,  $C_{MB}$ , have been approximated by the two first terms of their development in Taylor series at  $\alpha = 90^\circ$  and  $\gamma = 0^\circ$ . These coefficients are used to similar pier and bridge decks. Aerodynamic coefficients of piers and the box girder have been calculated according to *the European Standard EN 1991-1-4:2005*.

Table 1 Position of wind pressure center at the end of each time period

Section	Period (s)	$d_i^*$ (m)	Description
1	$0 - t_4$	7.9	The front bogie enters the wind zone.
2	$t_4 - t_5$	1.6	The rear bogie enters the wind zone.
3	$t_5 - t_1$	0.8	The vehicle enters the wind zone.
4	$t_1 - t_2$	0	The vehicle is immersed in the wind zone.
5	$t_2 - t_6$	-1.6	The front bogie lives the wind zone.
6	$t_6 - t_7$	-7.9	The rear bogie lives the wind zone.
7	$t_7 - t_3$	-9.5	The vehicle lives the wind zone.

\*where  $d_i$  are the distances between the wind pressure center and the shape center of car body at the end of each time period, which change with time during the vehicle entering or leaving the wind zone, and the distance of each integral time point is obtained by linear interpolation.

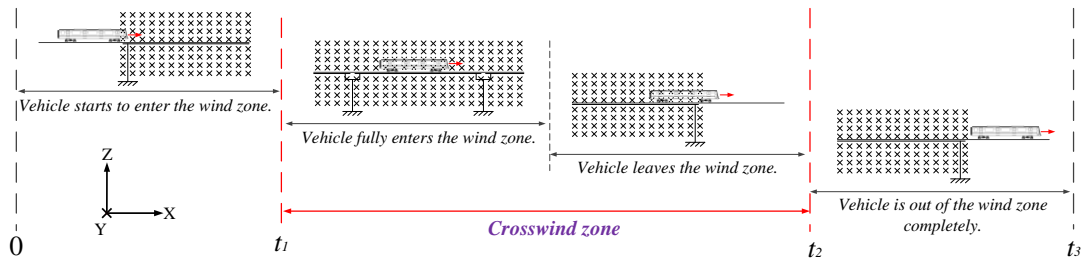


Fig. 10 Different stages of the vehicle crossing the crosswind zone

### 3.3 Crosswind load for metro vehicle

When metro vehicle enters or leaves crosswind zone, whose longitudinal positions change strongly with time. Then the change of the wind pressure centers is analyzed, the seven discrete wind pressure centers are selected, and the positions of crosswind pressure centers are determined. Furthermore, the corresponding wind pressure center positions at the end of each time period are determined, as shown in Fig. 10 and Table 1.

The crosswind forces and moments of the seven intervals is replaced by time-varying functions, and the position of wind pressure center at the end of each time period is shown in Table 1.

The vehicle is under crosswind with attack angle of  $\alpha$  and incoming wind velocity of  $U(t)$  (Xiang *et al.* 2018), as shown in Fig. 11.

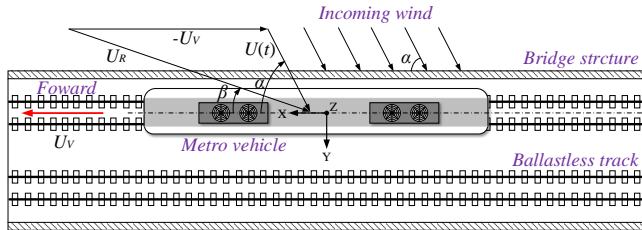


Fig. 11 The wind environment around the moving metro vehicle

The relative wind velocity  $U_R$  and the yaw angle  $\beta$  are

$$U_R = \sqrt{U(t)^2 + U_V^2 - 2U(t)U_V \cos(\pi - \alpha)} \tag{20}$$

$$= \sqrt{U(t)^2 + U_V^2 + 2U(t)U_V \cos(\alpha)}$$

$$\beta = \arctan[U(t) \sin \alpha / (U(t) \cos \alpha + U_V)] \tag{21}$$

where  $U_V$  is the car speed,  $U(t)$  is the incoming wind velocity,  $\alpha$  is the wind attack angle,  $\beta$  is the yaw angle,  $U_R$  is the air velocity relative to metro vehicle.

The aerodynamic coefficients are obtained from wind tunnel tests by Traction Power State Key Laboratory (Yu *et al.* 2012), the fitting formula are described as follows

$$\begin{cases} C_F = -0.1062 + 5.0535\beta + 2.4578\beta^2 \\ C_M = -0.3342 + 12.4329\beta - 10.0186\beta^2 \end{cases} \tag{22}$$

where  $C_F$ , and  $C_M$  are the force and moment coefficient of the car;  $\beta$  is the yaw angle.

The lateral force  $F_{wv}(t)$  and the yaw moment  $M_{wv}(t)$  for the car body during the period of the vehicle crossing the crosswind zone ( $t_1 \sim t_2$ ) can be described as

$$F_{wv}(t) = \begin{cases} \frac{t(t-2t_5)}{2t_1(t_1-2t_5)} + \frac{t(t-2t_4)}{2t_1(t_1-2t_4)} \cdot F_{wv0} & t \in (0, t_1) \\ F_{wv0} & t \in (t_1, t_2) \\ \frac{(t-t_3)(t+t_3-2t_7)}{2(t_2-t_3)(t_2+t_3-2t_7)} + \frac{(t-t_3)(t+t_3-2t_6)}{2(t_2-t_3)(t_2+t_3-2t_6)} \cdot F_{wv0} & t \in (t_2, t_3) \end{cases} \tag{23}$$

Table 2 Evaluation indices for the wind-train-bridge system

Item	Index	Logogram	Unit	Threshold value
Running stability index	Lateral Sperling index of car body	--	--	2.75
	Lateral acceleration of car body	--	g*	0.2
	Lateral force of wheel-rail	$Q$	kN	50
Running safety index	Derailment factor	$Q/P$	--	0.8
	Offload factor	$\Delta P / \bar{P}$	--	0.6
	Overturning factor	$D$	--	0.8
Bridge dynamic index	Lateral displacement of beam midspan	--	mm	7.5
	Lateral acceleration of beam midspan	--	m/s <sup>2</sup>	1.3
	Lateral displacement of the top of pier	--	mm	8.5
	Lateral acceleration of the top of pier	--	m/s <sup>2</sup>	--

\*where the 'g' is gravity acceleration (9.81m/s<sup>2</sup>).

$$M_{wv}(t) = \begin{cases} \frac{t(t-2t_3)}{2t_1(t_1-2t_3)} + \frac{t(t-2t_4)}{2t_1(t_1-2t_4)} \cdot F_{wv0} \cdot d_i & t \in (0, t_1) \\ M_{wv0} & t \in (t_1, t_2) \\ \frac{(t-t_3)(t+t_3-2t_7)}{2(t_2-t_3)(t_2+t_3-2t_7)} + \frac{(t-t_3)(t+t_3-2t_6)}{2(t_2-t_3)(t_2+t_3-2t_6)} F_{wv0} d_i & t \in (t_2, t_3) \end{cases} \quad (24)$$

$$\begin{cases} F_{wv0} = 0.5\rho S_v C_F U_R(t)^2 \\ M_{wv0} = 0.5\rho S_v H_v C_M U_R(t)^2 \end{cases} \quad (25)$$

where  $\rho$  is the air density (kg/m<sup>3</sup>),  $S_v$  is the effective windward area (m<sup>2</sup>),  $H_v$  is the distance between mass center of car and bridge (m).

Based on this, for instance, when the mean wind speed of standard height is 8 m/s, while vehicle speed is 80 km/h and the wind attack angle  $\alpha$  is 90<sup>0</sup>, the crosswind forces  $F_{wv}$  and the moment  $M_{wv}$  change with time are shown in Fig. 12, as follows

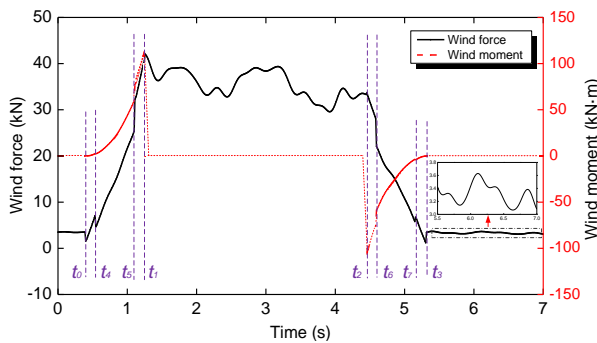


Fig. 12 Crosswind force and moment samples for car body

where  $t_3$  is the time when the vehicle completely leaves the crosswind zone;  $t_4$ ,  $t_5$  are the moments when the front and the rear bogies of the metro vehicle enter the crosswind zone, respectively;  $t_6$  and  $t_7$  are the departure moments, respectively.

#### 4. Characteristic analysis of the metro vehicle-bridge system with high-pier under crosswind

In this section, calculation parameters of metro vehicle, line, high-pier bridge and crosswind loads are determined, and the track irregularity excitation is correctly considered. Then, dynamic evaluation indices are selected according to the research needs. Meanwhile, response comparison of the dynamic system with crosswind and no-wind is analyzed, in which the response comparison of the dynamic system with high-pier and low-pier is analyzed.

##### 4.1 The evaluation indices for the dynamic system under crosswind

The components at high-pier bridge mid-span and car body in along-wind direction are mainly studied. Therefore, the safety and stability of the running train crossing bridge and dynamic performance of the bridge are three aspects that not be overlooked.

Lateral  $W_Y$  index calculate Sperling's running stability indices for lateral direction of car body (GB/T 50157-2013). Lateral Sperling index of car body are calculated as

$$W_Y = 10 \sqrt{\int_{0.5}^{30} a^3 B_w^3 df} \quad (26)$$

$$B_w = 0.737 \left[ \frac{1.911f^2 + (0.25f^2)^2}{(1 - 0.28f^2)^2 + (1.56f - 0.037f^3)^2} \right]^{\frac{1}{2}} \quad (27)$$

where  $a$  is acceleration in frequency domain (cm/s<sup>2</sup>),  $f$  is the frequency (Hz).

The lateral force of wheel-rail ( $Q$ ), the derailment factor ( $Q/P$ ) and offload factor ( $\Delta P/\bar{P}$ ) are three kinds of derailment safety indices, ( $\Delta P/\bar{P}$ ) is described as

$$\frac{\Delta P}{\bar{P}} = \frac{(P_{st1} + P_{st2})/2 - P_i}{(P_{st1} + P_{st2})/2} \quad (28)$$

where  $P$  is the vertical force of wheel-rail;  $P_{st1}$  and  $P_{st2}$  are the static wheel weight of left and right side wheels;  $P_i$  is the vertical force of the load reducing side wheel.

The overturning factors is used to identify whether the vehicle will capsize, which can be described as

$$D = P_d / P_{st} = (P_2' - P_1') / (P_2' + P_1') \quad (29)$$

where  $P_{st}$  is the vertical static load of wheel rail without lateral force;  $P_d$  is the change of vertical force under the action of transverse force;  $P_2'$  and  $P_1'$  are, respectively, vertical force of wheel rail on load side and load side.

To sum up, the evaluation indices and the corresponding threshold are selected according to GB/T 50157-2013: *Code for Metro Design*, as shown in Table 3.

#### 4.2 Calculation parameters of the dynamic system and crosswind load

Lots of calculation parameters should be determined to study the running safety of the dynamic system. Firstly, the high-pier viaduct is described as a three-span simply-supported girder bridge with four piers, whose names are shown in Fig. 6. The height of high-pier is 50 m and short-pier is 5 m, the cross section of the pier is 3 800 mm×2 000 mm, respectively, as shown in Fig. 13. The mean wind speed of standard height ( $z = 20$  m) is 8 m/s and the wind angle  $\alpha = 90^\circ$  and  $\gamma = 0^\circ$ , while train speed is 80 km/h.

Considering the actual conditions of the metro lines in Chongqing, the power spectrum of German low-speed track irregularity is adopted in this work (Zhai *et al.* 2011), which are shown in Fig. 14.

A typical metro vehicle is adopted in this work, whose parameters were provided by CRRC Qingdao Sifang Co., Ltd, as shown in Table 3.

#### 4.3 Responses comparison of the dynamic systems with crosswind and no-wind

Crosswind can trigger damage to bridges in many ways. Vibration of bridge deck may lead to traffic disruption or loss of safety for running train, lead to premature fatigue of bridge components and, in serious cases, lead to bridge destruction (Cai *at al.* 2015), which affects the dynamic system apparently, especially the piers are high. Therefore, it is significant to study the characteristics of the wind-vehicle-bridge system. The response is shown in Fig. 15.

As can be seen from Fig. 15, crosswind acts on the car body, the piers and the bridge decks, which triggers strong vibrations of vehicle and lateral deformation of the entire bridge.

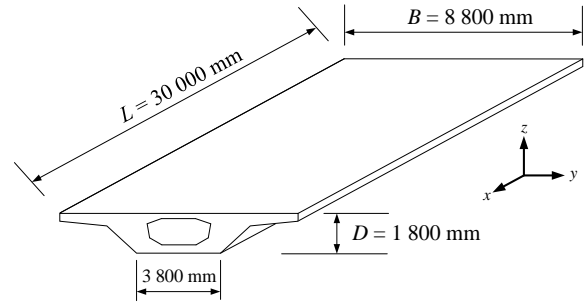
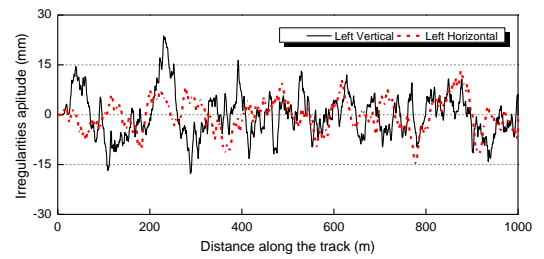
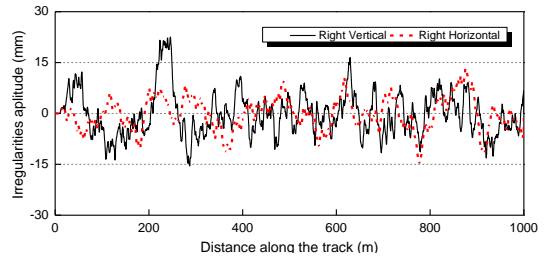


Fig. 13 Cross section of the bridge



(a) Vertical and horizontal irregularities of left rail



(b) Vertical and horizontal irregularities of right rail

Fig. 14 Samples of the power spectrum of German low-speed track irregularity

Table 3 Parameters of the metro vehicle

Item	Component	Value
Car body	Vehicle width	2 800 mm
	Vehicle height	3 695 mm
	Vehicle length	20 020 mm
	Vehicle base	12600 mm
	Car mass	35.443 t
	Height of car mass center	1 929 mm
Bogie	Frame mass	4.007 t
	Wheelset mass	1.878 t
	Wheel diameter	840 mm
	Wheel base	2300 mm
Suspension	Transverse span	1493 mm
	Primary suspension ( $k_{pz}$ )	0.34 MN/m
	Primary suspension ( $k_{pyy}$ )	0.22 MN/m
	Secondary suspension ( $k_{sz}$ )	0.34 MN/m
	Secondary suspension ( $k_{sxy}$ )	0.15 MN/m

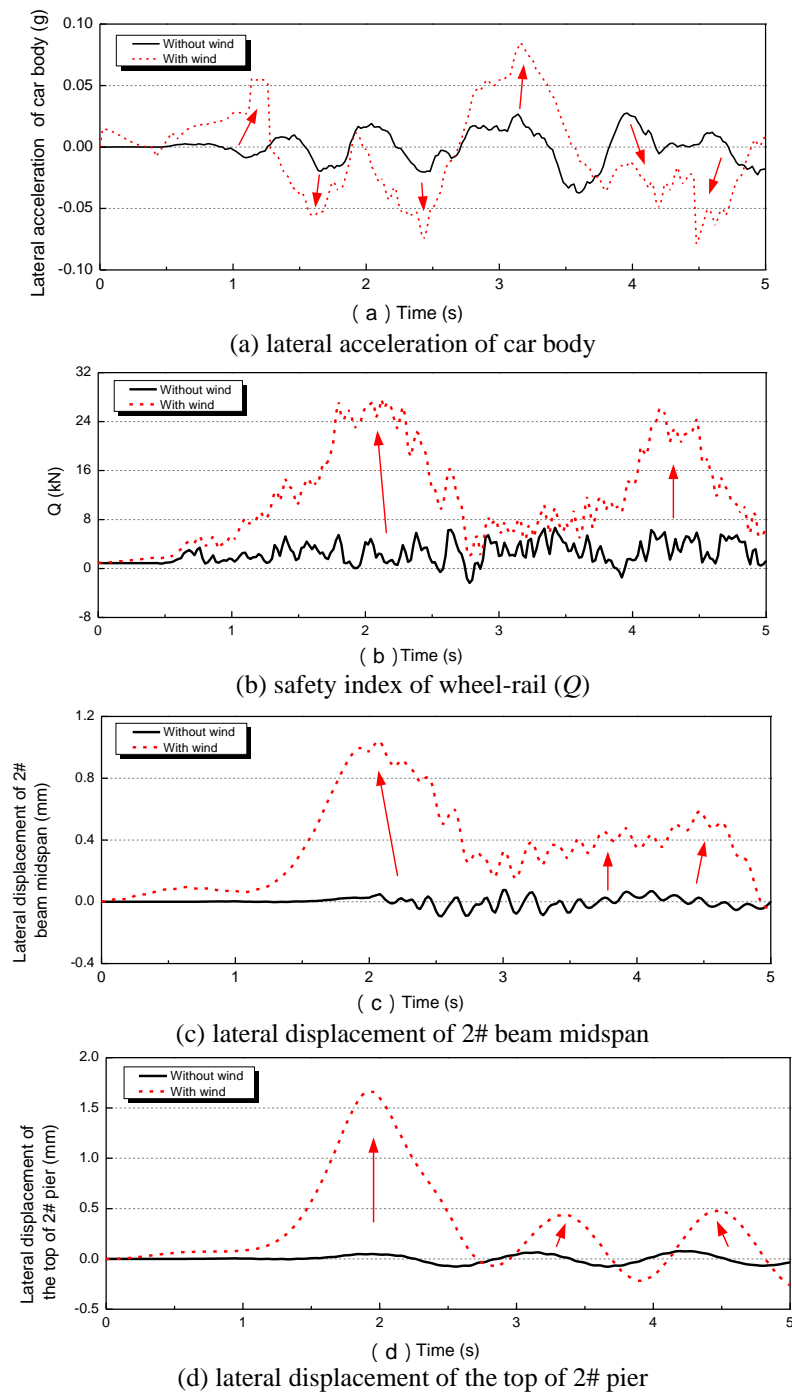


Fig. 15 Changes of response after loading crosswind

The yaw moment change during ( $t_0 \sim t_1$ ) and ( $t_2 \sim t_3$ ), while the car body is subjected to a strong torque due to enter and leave crosswind zone. It can be seen in Fig. 10, the vibration of the beam and pier are consistent between 0.4s and 1.2s, which is caused by vehicle entering crosswind zone. After loading crosswind, the amplitudes of all indices become larger than the condition of no-wind. That indicates that crosswind triggers larger response of the dynamic system and greater effect on the running safety of metro vehicle compared with the conditions of no-wind.

The yaw moment change during ( $t_0 \sim t_1$ ) and ( $t_2 \sim t_3$ ), while the car body is subjected to a strong torque due to enter and leave crosswind zone. It can be seen in Fig. 10, the vibration of the beam and pier are consistent between 0.4s and 1.2s, which is caused by vehicle entering crosswind zone. After loading crosswind, the amplitudes of all indices become larger than the condition of no-wind. That indicates that crosswind triggers larger response of the dynamic system and greater effect on the running safety of metro vehicle compared with the conditions of no-wind.

Table 4 Responses comparison of the wind-vehicle-bridge system with high-pier and short-pier

Item	Index	High-pier	Short-pier
Running stability index	Lateral Sperling index	2.70	2.20
	Lateral acceleration of car body ( $g^*$ )	0.10	0.05
	$Q/P$	0.31	0.17
Running safety index	$Q$ (kN)	27.97	11.95
	$D$	0.75	0.28
	$\Delta P/\bar{P}$	0.79	0.33
Bridge dynamic index	Lateral displacement of pier top (mm)	1.67	0.001
	Lateral displacement of beam midspan (mm)	1.05	0.16
	Lateral acceleration of pier top ( $m/s^2$ )	0.16	0.02
	Lateral acceleration of beam midspan ( $m/s^2$ )	0.20	0.15

\*where the 'g' is gravity acceleration ( $9.81m/s^2$ ).

#### 4.4 Responses comparison of the dynamic systems with high-pier and short-pier

Crosswind is stronger because of the distance increases between the deck and the ground. Compared with the short-pier bridge, the high-pier bridge has worse stability. In these lateral flexible bridges, the deck movements, induced by crosswind, can affect running safety aggravating the problem. Responses of the dynamic system with high-pier (50 m) and short-pier (5 m) are shown in Table 4.

As can be seen from Table 4, compared with short-pier bridge, the metro vehicle traveling on the high-pier bridge triggers stronger vibration of the bridge structure and car body, which in turn triggers running instability of metro train (Guo *et al.* 2010). The responses of the dynamic system increase with high-pier than that with short-pier.

### 5. Safety zone for metro vehicle traveling on high-pier viaduct under crosswind

The effect of vehicle speed and wind speed on running safety of the vehicle-bridge system under crosswind is analyzed in this section. According to the selected sensitive indices, safety zone of critical train speed versus mean wind speed of standard height is determined.

#### 5.1 Influence of metro vehicle speed

Crosswind load acts on car body and triggers vibration of the train directly, which affects the running stability of the car (Guo *et al.* 2010). Meanwhile, running train are moving loads for the dynamic system, and loading frequency changes with train speed. In order to explore the effect of vehicle speed, the train speed is 60 - 100 km/h, while the mean crosswind speed of standard height ( $z = 20$  m) is 8 m/s and the wind angle  $\alpha = 90^\circ$  and  $\gamma = 0^\circ$ . The maximum responses of the dynamic system change with train speed are shown in Fig. 16.

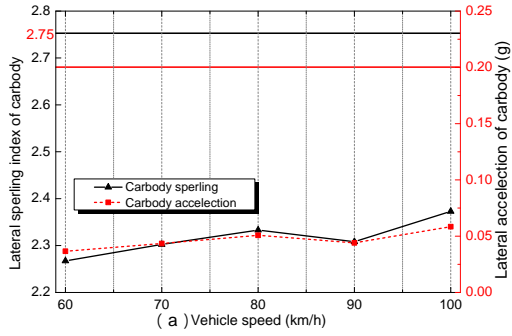
As can be seen in Fig. 16, the stability responses of the vehicle, the safety responses of wheel-rail and the dynamic responses of the high-pier bridge increase with the vehicle speed on the whole process. Furthermore, several abnormalities in the evaluation of car body and bridge vibration cannot be ignored. In particular, unusually large amplitude points occur at the vehicle speed 70 & 80 km/h.

The running vehicle is a moving load for the dynamic system, loading frequency changes with the vehicle speed (Guo *et al.* 2010). Assuming that the vehicle over the viaduct at a speed  $v$ , while that is equivalent to applying a periodic load of frequency  $f_v = v/L$  to the bridge structure. For these reasons, the corresponding dynamic load frequencies for vehicle speed of 60 km/h, 70 km/h, 80 km/h, 90 km/h and 100 km/h are 0.556 Hz, 0.648 Hz, 0.741 Hz, 0.833 Hz and 0.926 Hz, respectively. In the meantime, the lateral natural vibration frequencies of the high-pier bridge are 0.648 Hz (the yaw natural vibration frequency of metro vehicle), 0.783 Hz (the lateral oscillation vibration frequency of the high-pier) and 0.961Hz (the horizontal swing natural vibration frequency of the beam), respectively. These loading frequencies are close to the natural vibration frequency so that resonance occurs, which triggers each structure transmits violent vibrations to each other and the indices increase sharply.

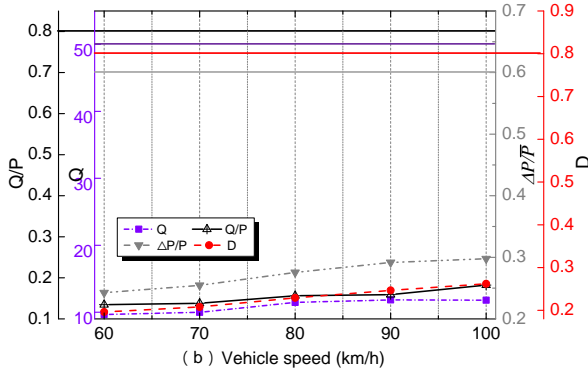
#### 5.2 Influence of crosswind speed

In order to explore the effect of wind speed and the corresponding threshold, the vehicle speed is 80 km/h (22.22 m/s), while mean crosswind speed of standard height ( $z = 20$  m) are 5 - 28 m/s and the wind angle  $\alpha = 90^\circ$  and  $\gamma = 0^\circ$ , and other parameters are unchanged. The maximum responses of the vehicle-bridge system change with wind speed are shown in Fig. 17.

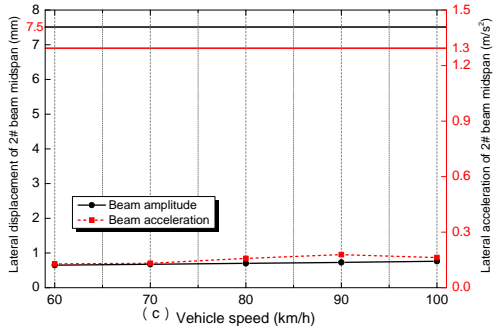
It can be seen in the calculation results, lateral Sperling index value of car body, lateral acceleration of car body,  $\Delta P/\bar{P}$  and  $D$  exceed the limits. While others are not to reach the safety limit, whose regularity are nearly consistent so that they are not shown in this work. The maximum responses of the vehicle-bridge system change with wind speed are shown in Fig. 17.



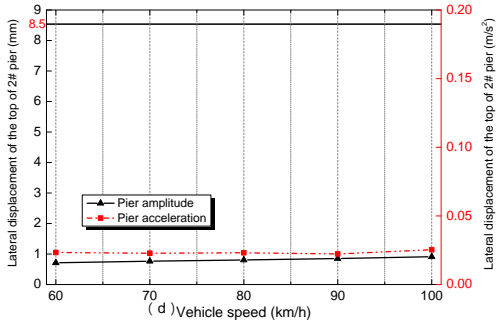
(a) The stabilities of running vehicle



(b) The safeties of running vehicle



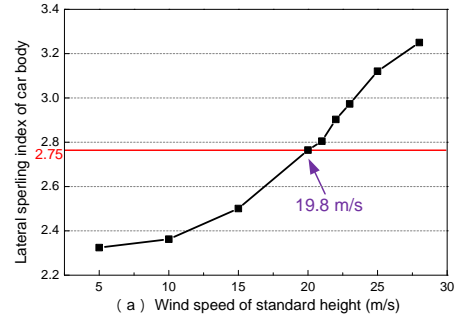
(c) The dynamics performance of the beam



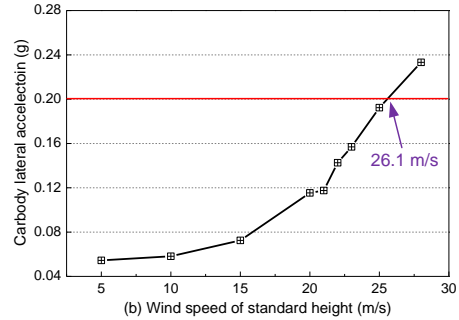
(d) The dynamics performance of the high-pier

Fig. 16 The response changes of the vehicle-bridge system with vehicle speed

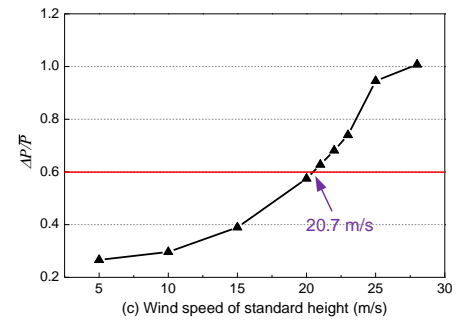
From the figures, it can also be seen that the maximum response of running train on the high-pier bridge increases to varying degrees with wind speed. Further, the dynamic response of metro train is more sensitive to the change of wind speed than bridge structure. Even if the index value of the bridge does not reach the limit value, the vehicle stability index and safety index exceed the safety limit,



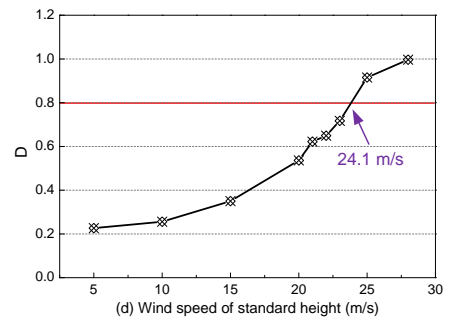
(a) Lateral Spurling index of car body



(b) Lateral acceleration of car body



(c) Offload factor ( $\Delta P/\bar{P}$ )



(d) Overturning factor ( $D$ )

Fig. 17 The changes of the dynamic system with crosswind speed

which is very dangerous. The critical speed of lateral Spurling index of car body, lateral acceleration of car body, overturning factor ( $D$ ) and offload factor ( $\Delta P/\bar{P}$ ) are 19.8 m/s (2.75), 26.1 m/s (0.2 g), 24.1 m/s (0.8) and 20.7 m/s (0.6).

The results show that when the mean wind speed of standard height reaches 19.8 m/s and the train speed is 80 km/h, lateral Spurling index of car body exceeds its limit

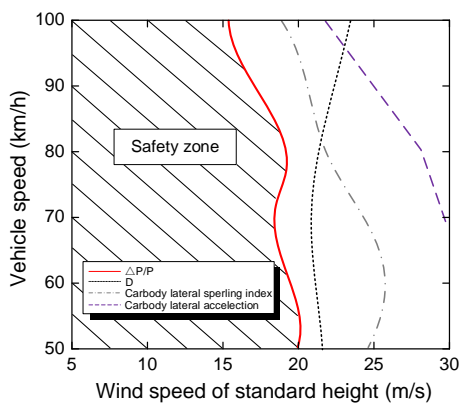


Fig. 18 Safety zone for the vehicle-bridge system under crosswind

(2.75), indicating the running safety of the train on the bridge cannot be guaranteed.

### 5.3 Safety zone for metro vehicle-bridge system with high-pier viaduct under crosswind

It can be noticed that the running safety indices increase significantly with mean wind speed, whereas appear to fluctuations with train speed. To ensure the running safety of metro train over the high-pier bridge, it is necessary to strictly limit the train speed under various wind speeds. The train speed is 50 - 100 km/h, while mean crosswind speed of standard height ( $z = 20$  m) are 5 - 30 m/s and the wind angle  $\alpha = 90^\circ$  and  $\gamma = 0^\circ$ . The threshold speed of a train traveling on the bridge under crosswinds is determined, as shown in Fig. 18.

As can be seen from Fig. 18, the red curve shows the boundary between the safety zone and the dangerous zone. For instance, as the mean wind speed of standard height reaches 22 m/s, the critical train speed is around 50 km/h, indicating the metro traffic on the high-pier bridge should not exceed the corresponding limited vehicle speed to ensure the running safety.

## 6. Conclusions

Dynamic analysis of metro vehicle traveling on a high-pier viaduct under crosswind in mountain city has been studied in this paper. In the first place, a dynamic model of the metro vehicle-track-bridge system under crosswind is built, then crosswind loads model considering the condition of wind zone has been established. After that, the evaluation indices and the calculation parameters have been selected, based on this, the basic characteristics of the dynamic system with high-pier under crosswind have been analyzed.

Moreover, the response varies with vehicle speed and wind speed have been calculated, thereupon, the safety zone has been determined. Some conclusions could be drawn on the basis of above calculation analysis:

- The conditions of wind zone and the factor of high-pier bridge play essential roles that cannot be ignored in ensuring the running safety of the metro vehicle traveling on the high-pier viaduct under crosswind in mountain city.
- Compared with the conditions of no-wind, crosswind triggers severer vibration of the dynamic system; besides, compared with the short-pier bridge, the high-pier bridge has worse stability under crosswind, which in turn causes running instability of the metro train.
- The running safety indices increase significantly with mean wind speed, whereas appear to fluctuations with train speed; on this basis, the safety zone is determined to ensure the running safety of metro train.

In the further work, more reasonable conditions will be adopted to further analyze running safety of metro train-bridge system in mountain city.

## Acknowledgments

The research described in this paper was financially supported by the National Natural Science Foundation of China (Grant number: 51405048), the open research fund of MOE Key Laboratory of High-speed Railway Engineering (Grant number: 2017-HRE-01), the Basic Natural Science and Frontier Technology Research Program of the Chongqing Municipal Science and Technology Commission (Grant number: stc2018jcyjAX0271), the open research fund of Chongqing Key Laboratory of Railway Vehicle System Integration and Control (Grant number: CKLURTSIC-KFKT-201804), the Chongqing Research Program of Frontier and Application Foundation (Grant number: cstc2018jcyjAX0087) and the Project of Fund Cultivation of Chongqing Jiaotong University [Grant number: 2018PY14].

## References

- Cai, C.B., He, Q.L., Zhu, S.Y., Zhai, W.M. and Wang, M.Z. (2019), "Dynamic interaction of suspension-type monorail vehicle and bridge: numerical simulation and experiment", *Mech. Syst. Signal Pr.*, **118**, 388-407.
- Cai, C.S., Hu, J.X., Chen, S., Han, Y., Zhang, W. and Kong, X. (2015), "A coupled wind-vehicle-bridge system and its applications: a review", *Wind Struct.*, **20**(2), 117-142. <http://dx.doi.org/10.12989/was.2015.20.2.117>.
- Cheli, F., Ripamonti, F., Sabbioni, E. and Tomasini, G. (2011), "Wind tunnel tests on heavy road vehicles: Crosswind induced loads - Part 2", *J. Wind Eng. Ind. Aerod.*, **99**(10), 1011-1024. <https://doi.org/10.1016/j.jweia.2011.07.007>.
- Chen, N., Li, Y.L., Wang, B., Su, Y. and Xiang, H.Y. (2015), "Effects of wind barrier on the safety of vehicles driven on bridges", *J. Wind Eng. Ind. Aerod.*, **143**, 113-127. <https://doi.org/10.1016/j.jweia.2015.04.021>.
- Chen, Z.W., Fang, H., Han, Z.L. and Sun, S.Z. (2019), "Influence of bridge-based designed TMD on running trains", *J. Vib. Control*, **25**(1), 182-193. <https://doi.org/10.1177/1077546318773022>.
- Chen, Z.W., Han, Z.L., Zhai, W.M. and Yang, J.Z. (2019), "TMD design for seismic vibration control of high-pier bridges in

- Sichuan–Tibet Railway and its influence on running trains”, *Vehicle Syst. Dyn.*, **57**(2), 207-225. <https://doi.org/10.1080/00423114.2018.1457793>.
- Guo, W.W., Xia, H. and Xu, Y.L. (2010), “Running safety analysis of a train on the Tsing Ma Bridge under turbulent winds”, *Earthq. Eng. Eng. Vib.*, **9**(3), 307-318.
- Guo, W.W., Xia, H., Karoumi, R., Zhang, T. and Li, X.Z. (2015), “Aerodynamic effect of wind barriers and running safety of trains on high-speed railway bridges under cross winds”, *Wind Struct.*, **20**(2), 213-236. <http://dx.doi.org/10.12989/was.2015.20.2.213>.
- He, X.H., Shi, K., Wu, T., Zou, Y.F., Wang, H.F. and Qin, H.X. (2016), “Aerodynamic performance of a novel wind barrier for train-bridge system”, *Wind Struct.*, **23**(3), 171-189. <http://dx.doi.org/10.12989/was.2016.23.3.171>.
- Li, X.Z., Wang, M., Xiao, J., Zou, Q.Y. and Liu, D.J. (2014), “Experimental study on aerodynamic characteristics of high-speed train on a truss bridge: A moving model test”, *J. Wind Eng. Ind. Aerod.*, **179**, 26-38. <https://doi.org/10.1016/j.jweia.2018.05.012>.
- Li, Y.L., Xiang, H.Y., Wang, B., Xu, Y.L. and Qiang, S.Z. (2013), “Dynamic analysis of wind-vehicle-bridge coupling system during the meeting of two trains”, *Adv. Struct. Eng.*, **16**(10), 1663-1670. <https://doi.org/10.1260/1369-4332.16.10.1663>.
- Ministry of housing and urban-rural development of PRC. (2013), *Code for design of metro GB/T 50157-2013*, China Building Industry Press, Beijing (in Chinese).
- Ministry of Railways of PRC. (2005), *Fundamental code for design on railway bridge and culvert TB 10002.1-2005*, China Railway Publishing House, Beijing (in Chinese).
- Niu, J.Q., Zhou, D., Liu, T.H. and Liang, X.F. (2017), “Numerical simulation of aerodynamic performance of a couple multiple units high-speed train”, *Vehicle Syst. Dyn.*, **55**(5), 681-703. <https://doi.org/10.1080/00423114.2016.1277769>.
- Olmos, J.M. and Astiz, M.Á. (2018), “Improvement of the lateral dynamic response of a high pier viaduct under turbulent wind during the high-speed train travel”, *Eng. Struct.*, **165**, 368-385. <https://doi.org/10.1016/j.engstruct.2018.03.054>.
- Olmos, J.M. and Astiz, M.Á. (2018), “Non-linear vehicle-bridge-wind interaction model for running safety assessment of high-speed trains over a high-pier viaduct”, *J. Sound Vib.*, **419**, 63-89. <https://doi.org/10.1016/j.jsv.2017.12.038>.
- Proppe, C., and Zhang, X.Y. (2015), “Influence of uncertainties on crosswind stability of vehicles”, *Science Direct*, **13**, 98-107. <https://doi.org/10.1016/j.piutam.2015.01.006>.
- Weinman, K.A., Fragner, M., Deiterding, R., Heine, D., Fey, U., Braenstroem, F., Schultz, B. and Wagner, C. (2018), “Assessment of the mesh refinement influence on the computed flow-fields about a model train in comparison with wind tunnel measurements”, *J. Wind Eng. Ind. Aerod.*, **179**, 102-117. <https://doi.org/10.1016/j.jweia.2018.05.005>.
- Xiang, H.Y., Li, Y.L., Chen, S.R. and Hou, G.Y. (2018), “Wind loads of moving vehicle on bridge with solid wind barrier”, *Eng. Struct.*, **156**, 188-196. <https://doi.org/10.1016/j.engstruct.2017.11.009>.
- Yu M., Zhang, J. and Zhang, W. (2012), “Running safety of high-speed trains on bridges under strong crosswinds”, *J. Mech. Eng.*, **48**(18), 104-111. (in Chinese)
- Zhai, W.M. (1996), “Two simple fast integration methods for large-scale dynamic problems in engineering”, *Int. J. Numer. Methods Eng.*, **39**(24), 4199-4214.
- Zhai, W. and Xia, H. (2011), “Train-track-bridge Dynamic Interaction: Theory and Engineering Application”, Science Press, Beijing (In Chinese).
- Zhai, W. and Zhao, C. (2016), “Frontiers and challenges of sciences and Technologies in Modern Railway Engineering”, *J. Southwest Jiaotong Univ.*, **51**(2), 209-226 (In Chinese with English abstract).
- Zhai, W., Wang, K. and Cai, C. (2009), “Fundamentals of vehicle-track coupled dynamics”, *Vehicle Syst. Dyn.*, **47**(11), 1349-1376. <https://doi.org/10.1080/00423110802621561>.
- Zhai, W., *et al.* (2013), “High-speed train-track-bridge dynamic interactions part I: theoretical model and numerical simulation”, *Int. J. Rail Transp.*, **1**(1-2), 3-24. <https://doi.org/10.1080/23248378.2013.791498>.

FR